Supplementary Information

Covalently bonded three-dimensional carbon nanotube solids via boron induced nanojunctions

Daniel P. Hashim[1], Narayanan T. Narayanan[1], Jose M. Romo-Herrera2, David A. Cullen[3], Myung Gwan Hahm[1], Peter Lezzi[4], Joseph R. Suttle[5], Doug Kelkhoff[6], E. Muñoz-Sandoval[7#], Sabyasachi Ganguli[8], Ajit K. Roy[8], David J. Smith[9], Robert Vajtai[1], Bobby G. Sumpter[10], Vincent Meunier[11], Humberto Terrones[10, 12], Mauricio cTerrones[13*], Pulickel M. Ajayan[1*]

[1] Department of Mechanical Engineering & Materials Science, Rice University, Houston, TX
[2] Departamento de Química Física and Unidad Asociada CSIC Universidade de Vigo, Campus Universitario, Vigo 3610, Spain
[3] Materials Science & Technology Division, Oak Ridge National Laboratory, Oak Ridge, TN 37831
[4] Department of Materials Science Engineering, Rensselaer Polytechnic Institute, Troy, NY
[5] Department of Physics, Rice University, Houston, TX
[6] Department of Materials Science Engineering, University of Illinois at Urbana-Champaign
[7] Instituto de Microelectrónica de Madrid, IMM (CNM-CSIC), Newton 8, Tres Cantos, Spain.
[8]Air Force Research Laboratory, 2941 Hobson Way, WPAFB, Dayton, OH 45433-7750, USA
[9]Department of Physics, Arizona State University, Tempe, AZ 85287
[10]Center for Nanophase Materials Sciences, Oak Ridge National Lab, One Bethel Valley Road, Oak Ridge, TN 37831-6487, USA
[11]Rensselaer Polytechnic Institute, Department of Physics, Applied Physics & Astronomy, Troy, NY 12180 USA
[12]UniversitéCatholique de Louvain, Institute of Condensed Matter and Nanosciences, Place Croix du Sud 1 (PCPM, Boltzmann) 1348 Louvain La Neuve, Belgium.
[13] Department of Physics, Department of Materials Science and Engineering & Materials Research Institute, The Pennsylvania State University, 104 Davey Lab., University Park, PA 16802-6300, USA & Research Center for Exotic Nanocarbons (JST), Shinshu University, Wakasato 4-17-1, Nagano-city 380-8553, Japan

*Corresponding author e-mails: ajayan@rice.edu, mut11@psu.edu

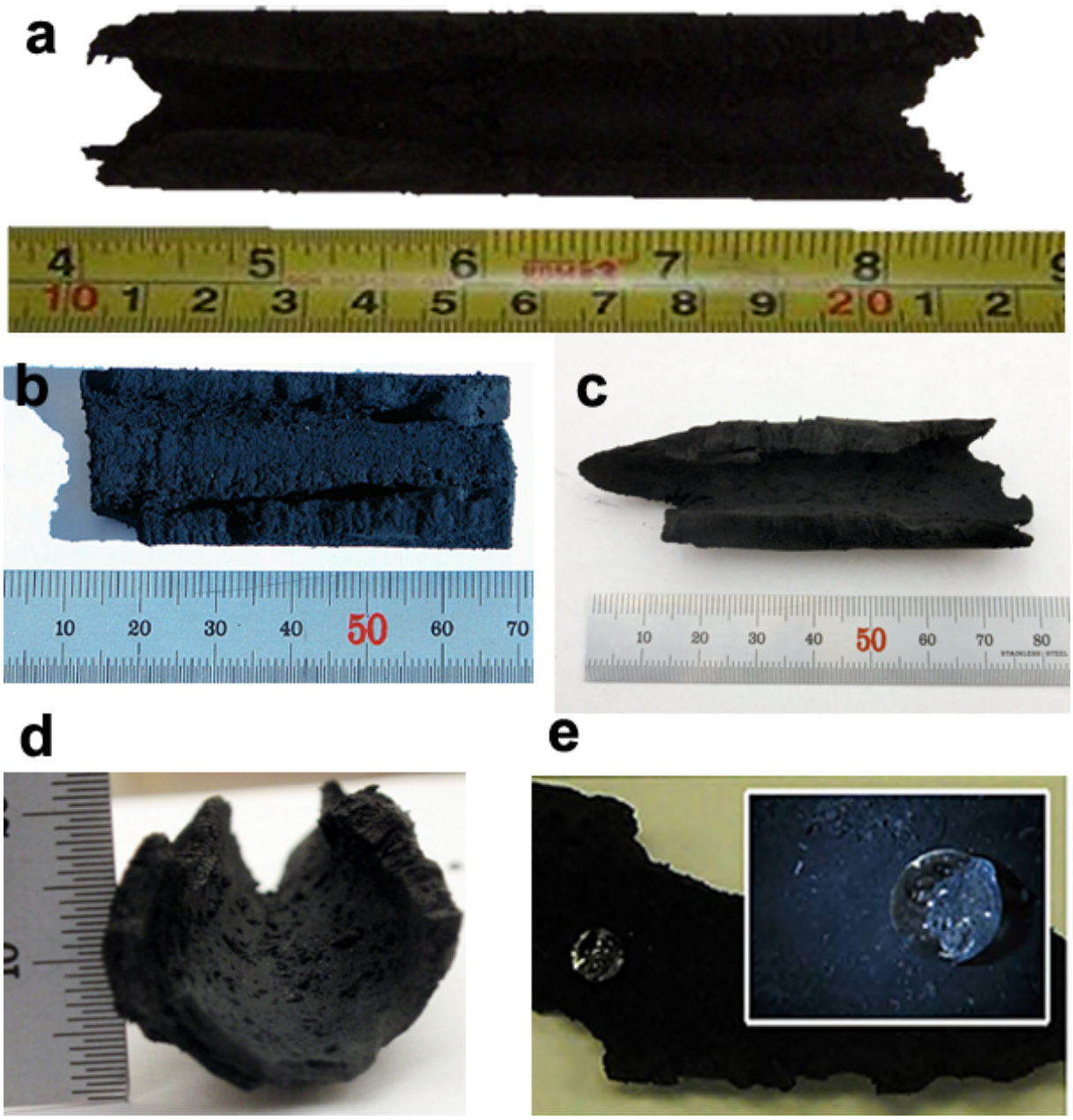

Fig. S1 Photographs of CBxMWNT macrostructures. (a) ;(b) photograph of a sponge taken under sunlight; (c) and (d) more sponge samples taking on the contoured shape of the 1 inch diameter quartz tube and (e) a water droplet beads-up on contact with the sponge surface indicative of its superhydrophobicity.

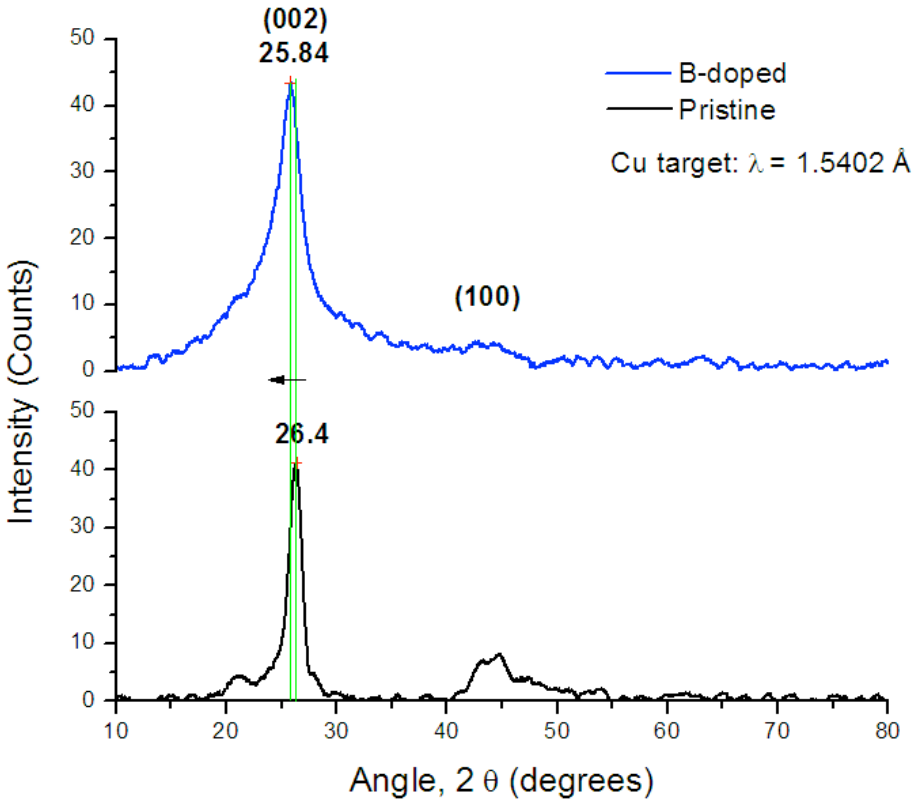

Fig. S2 X-Ray Diffraction patterns. The (002) peak location and width corresponds to the interlayer spacing of the concentric graphitic multi-walls. For the pristine (un-doped) MWCNTs (black) the (002) peak is at $2\boldsymbol{\theta}$ = 26.40º, which calculates to a lattice spacing, d = 3.37 Å. For our samples, the (002) peak seems to downshift to a lower angle for the CBxMWNT's spectrum (blue) to $2\boldsymbol{\theta}$ = 25.84º corresponding to a lattice spacing, d = 3.34 Å. This data shows the doped sample to have a more accurate spacing to the theoretically correct value of 3.4 Å and corresponds to a Δd = 0.07 Å. This may be a result of the presence of boron within the lattice which is known to enhance crystallinity [1], [2]. The (100) peak is related to the in-plane crystallinity of the layers. Certainly some peak broadening of the (002) planes appeared for B-doped samples. However, as compared to the pristine MWCNTs (black) there is no evidence of B_4C phase.

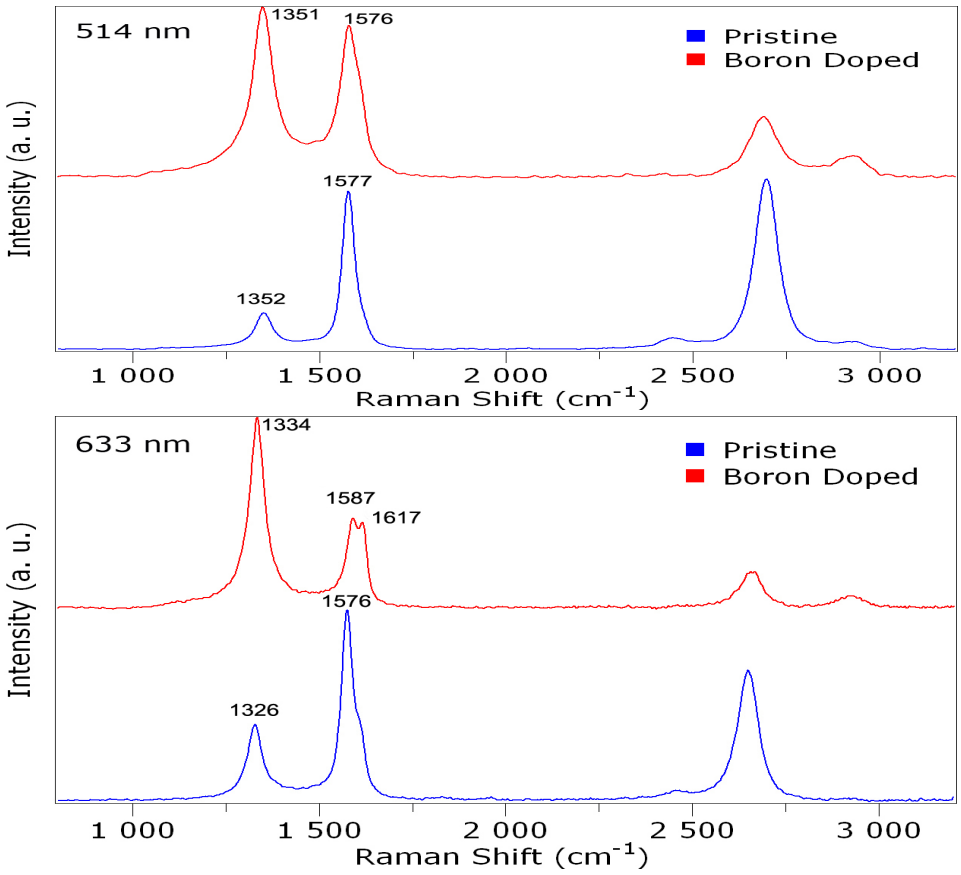

Fig. S3 Raman spectroscopy. Comparison of pristine MWCNT with CBxMWNT "sponge" were made using 514nm and 633nm wavelength laser. There is evidence of a stronger D-peak intensity compared to the G-peak intensity due to the dramatic structural defects formed by the presence of boron in the hexagonal carbon network. The splitting in the G peak is indeed due to the introduction of boron and this peak is known as the D' peak. Once boron is added within the lattice of graphene sheets, the perfect hexagonal symmetry of the sheets is broken and also the D band is increased, as well as the presence of the D', which is seen as the splitting of the G band. Thus, the strong defect-induced peaks (D- and D'-bands) originate from the substitutional boron atoms in graphene. These results are similar to those previously reported for boron doping in graphite, SWCNTs and MWCNTs [3]-[8]. The Raman features of the boron-doped sample are also similar to that of the defective graphene prepared by ion bombardment, at 1013 Ar^{+}/cm^{2} [9].

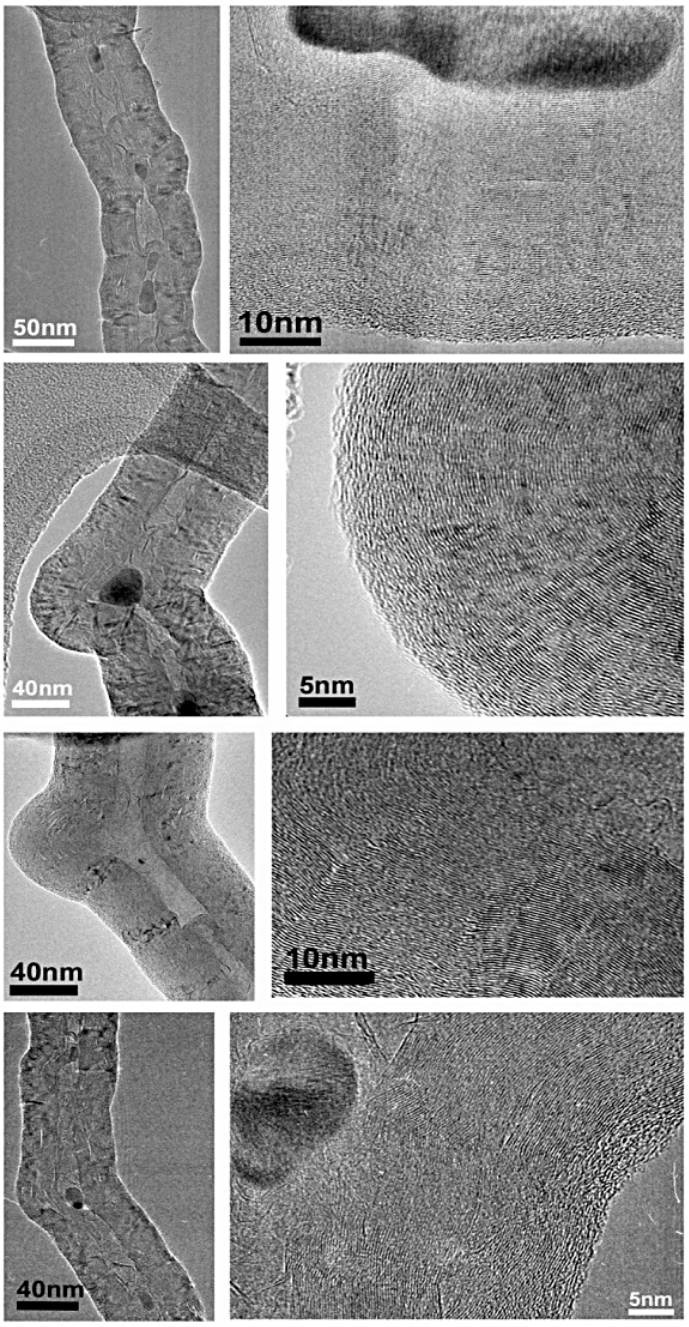

Fig. S4 High resolution transmission electron microscopy (HRTEM). Some more images of the "elbow" defects and extreme lattice curvature witnessed in the CB_XMWNTs.

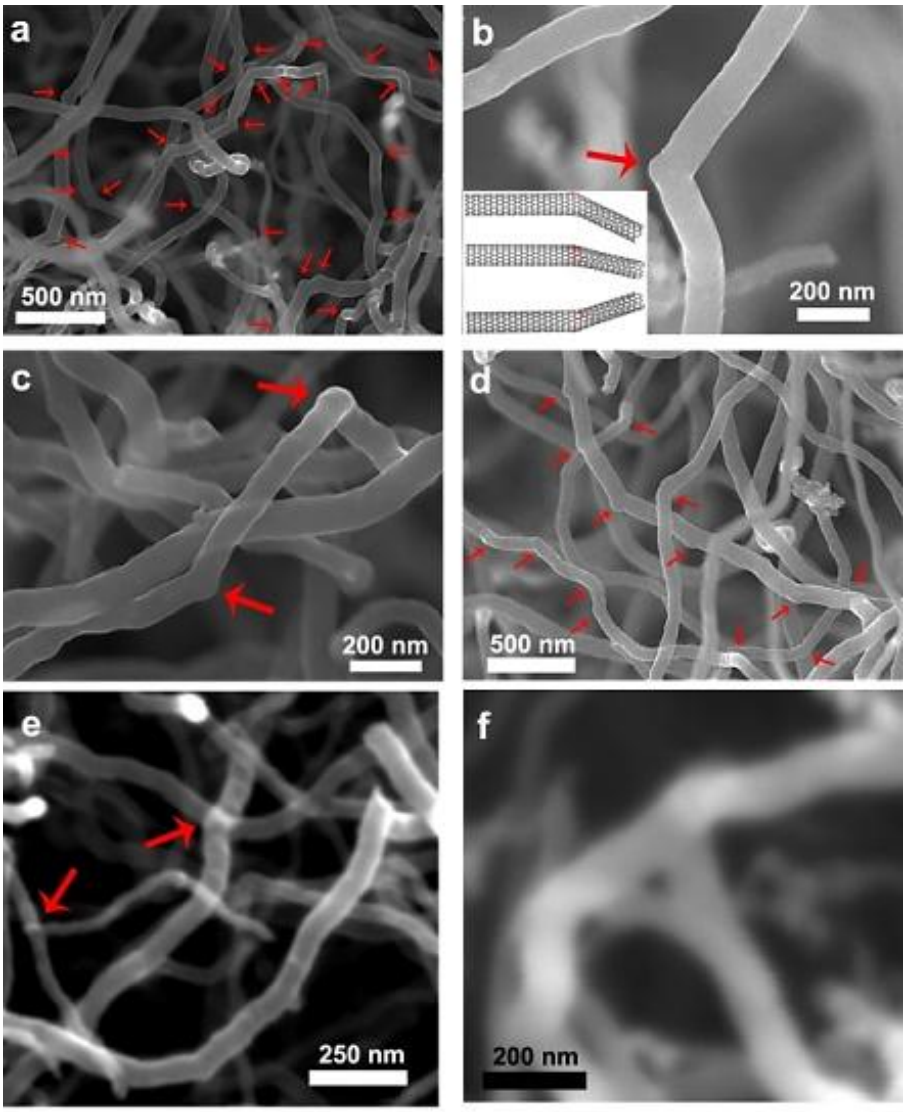

Fig. S5 More SEM characterization of "elbow" and junctions. More SEM images of the elbow nanojunctions (indicated by white arrows) found in CBxMWNT's. Inset (B) shows a computer generated model of different views of the pentagon-heptagon pair (in red) induced by the presence of boron in the nanotube lattice (note the change in chirality of the tubes). (D) Elbow defects occur continuous and somewhat at periodic distance intervals along the tube length of an individual CBxMWNT.

(a)

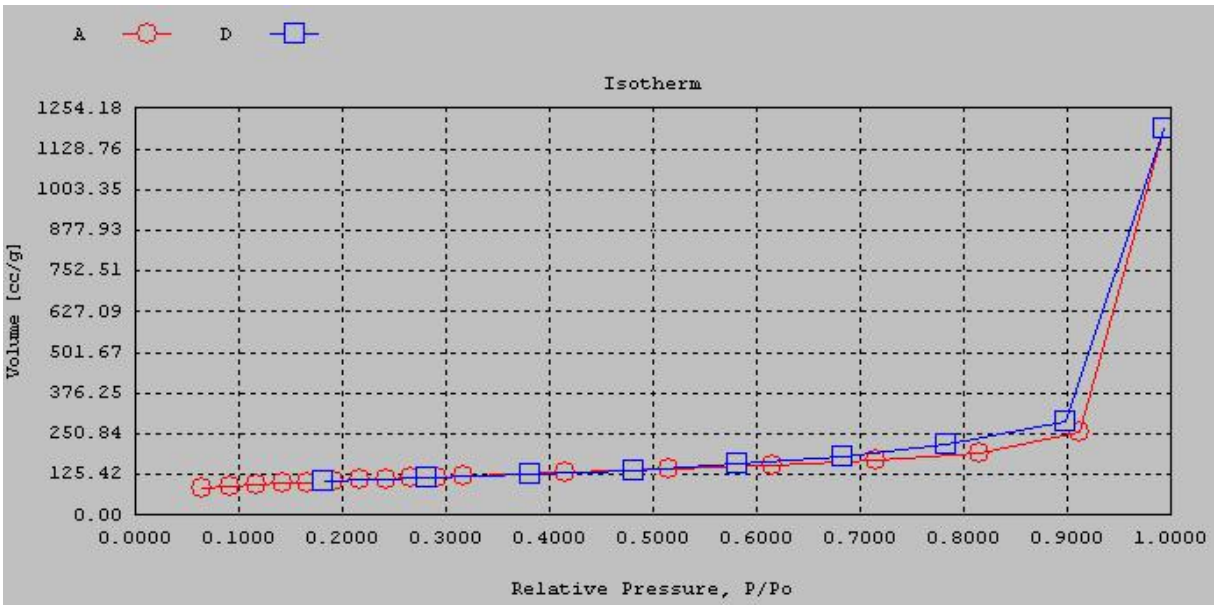

(b)

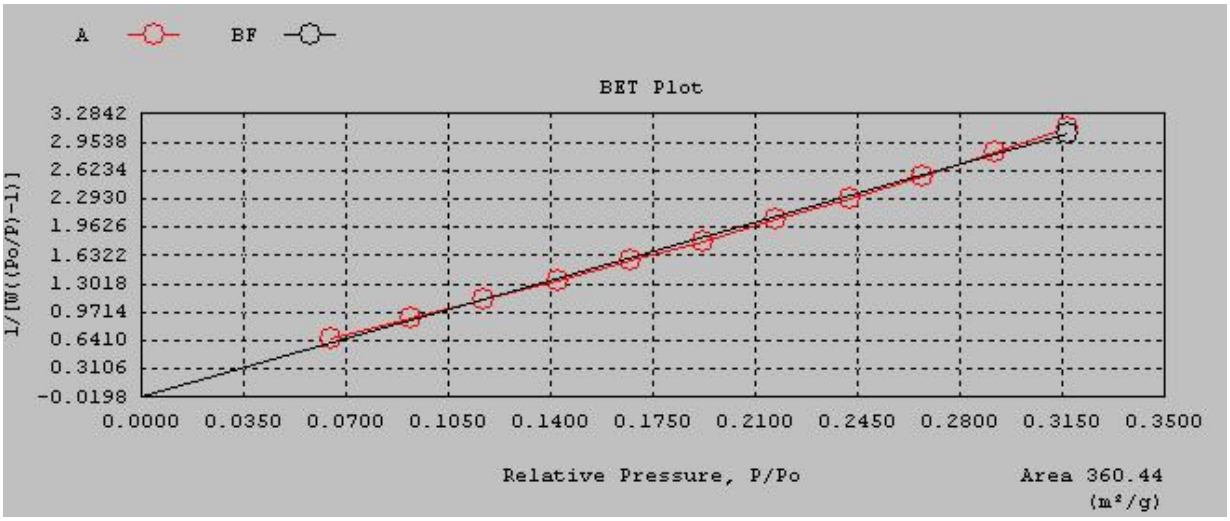

Fig. S6 BET surface area and porosity. (a) The N_2 absorption isotherm shows a type-II adsorption isotherm that exhibits a negligible concave section, which is known to be attributed to microporous volume uptake, and a rapid rise in total volume near $P/P_0 = 1$ indicating a macroporous material; (b) BET surface area, S_{BET}, shows to be 360.44 m^2/g.

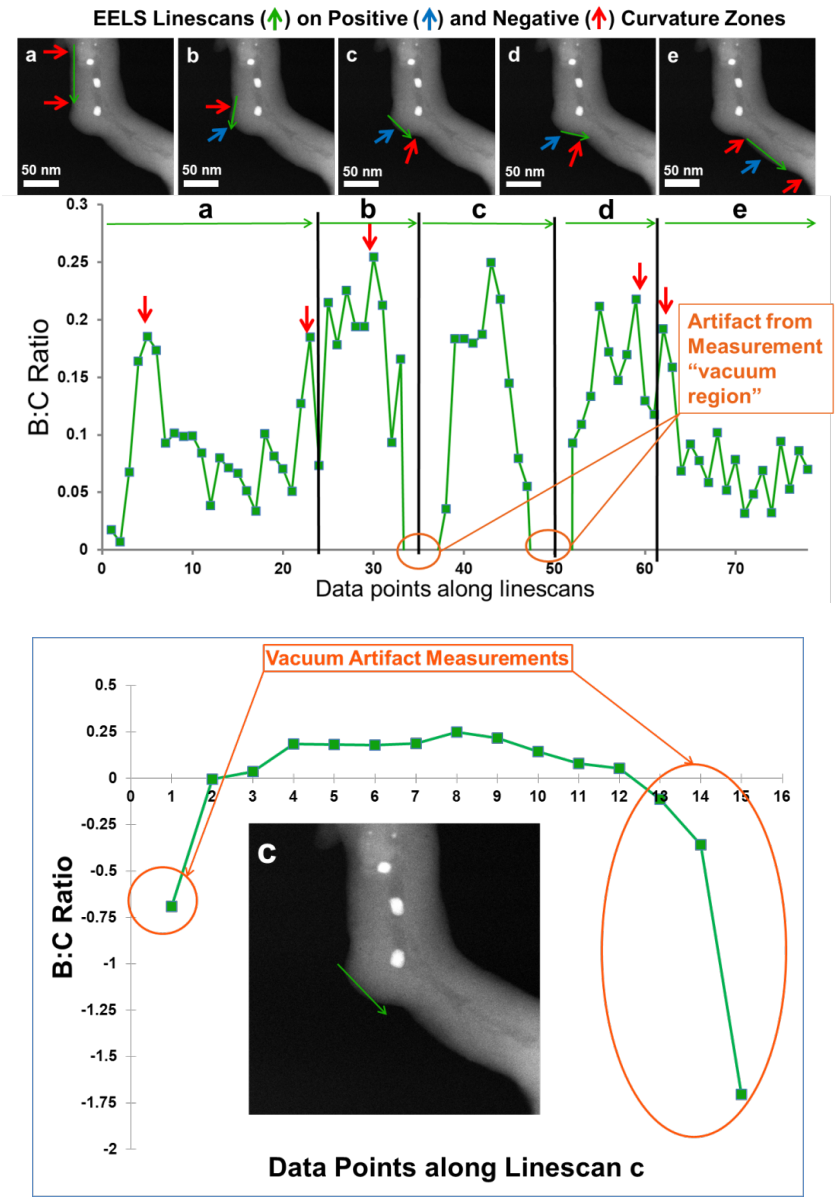

Fig. S7 More EELS linescans. SEM image showing EELS linescans a-e (green arrows) performed along the positive (blue arrows) and negative (red arrows) curvature regions on the "elbow" defect side. The corresponding B:C ratio from the EELS linescans a-e are labeled and represented by the green data points. The red arrows point to the peaks near the negative curvature regions surronding the positive curvature regions along the "elbow" bend. The orange circles indicate where the linescans extend into the "vacuum region" representing artifacts from the measurement.

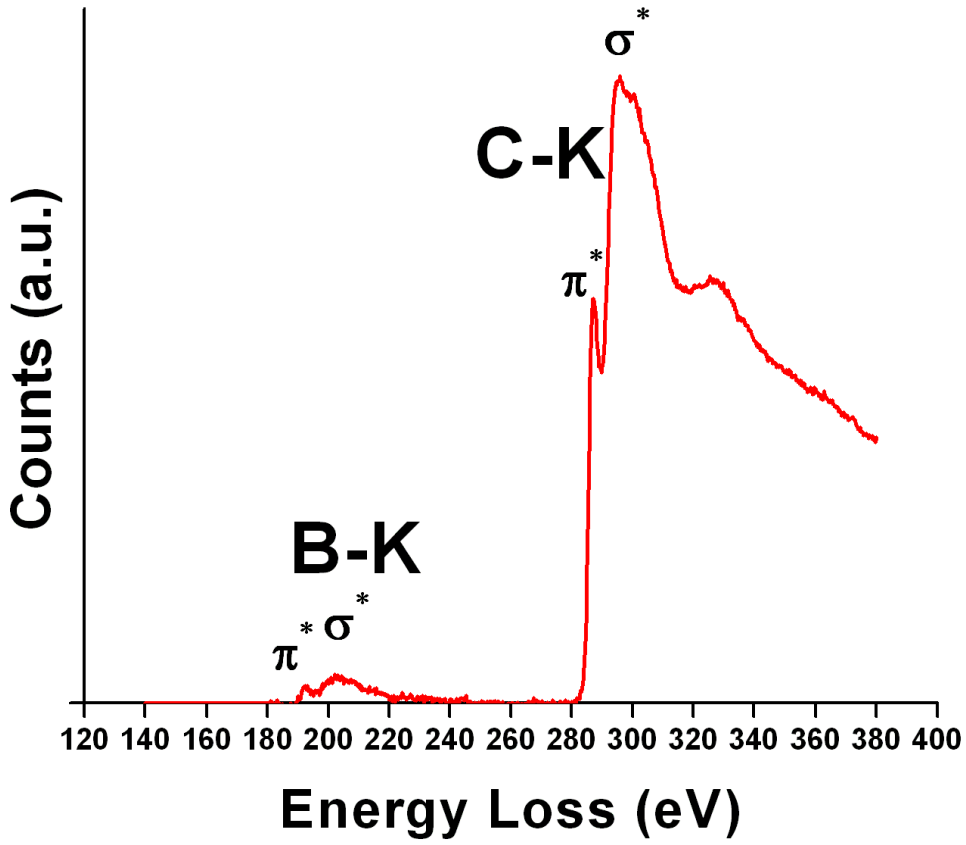

Fig. S8 EELS Elemental Survey Scan. The backround subtracted EELS spectrum of the CBxMWNT's showing both the C and B characteristic K-shell peaks. The C K-edge shows maximum peaks at 287.2 and 295.4 eV which correspond to the 1s π^* and 1s σ^* resonance respectively. Meanwhile, the B K-edge shows maximum peaks at 193.2 and 202 eV corresponding to the 1s π^* and 1s σ^* resonance respectively. The 1s π^* resonance is indicative of sp^2 hybridization, which indicates that boron is bonded to carbon within the carbon nanotube lattice.

Solvent	Sponge ρ = 24.3 mg/cc	Sponge ρ = 17.3 mg/cc	Sponge ρ = 10.8 mg/cc
Hexanes (0.6548 g/ml)	26.00	29.61	44.37
Ethanol (0.789 g/ml)	30.65	33.14	62.61
Kerosene (0.81 g/ml)	31.99	36.81	59.29
Toluene (0.867 g/ml)	37.38	48.46	65.48
Used Engine Oil (0.913 g/ml)	41.06	54.45	78.85
Ethylene Glycol (1.1132 g/ml)	52.98	74.38	79.526
Chloroform (1.483 g/ml)	62.28	76.91	122.86

Table S1 Solvent/oil absorption data. It is obvious that increasing solvent density and decreasing sponge density results in higher absorption capacity (g g^{-1}).

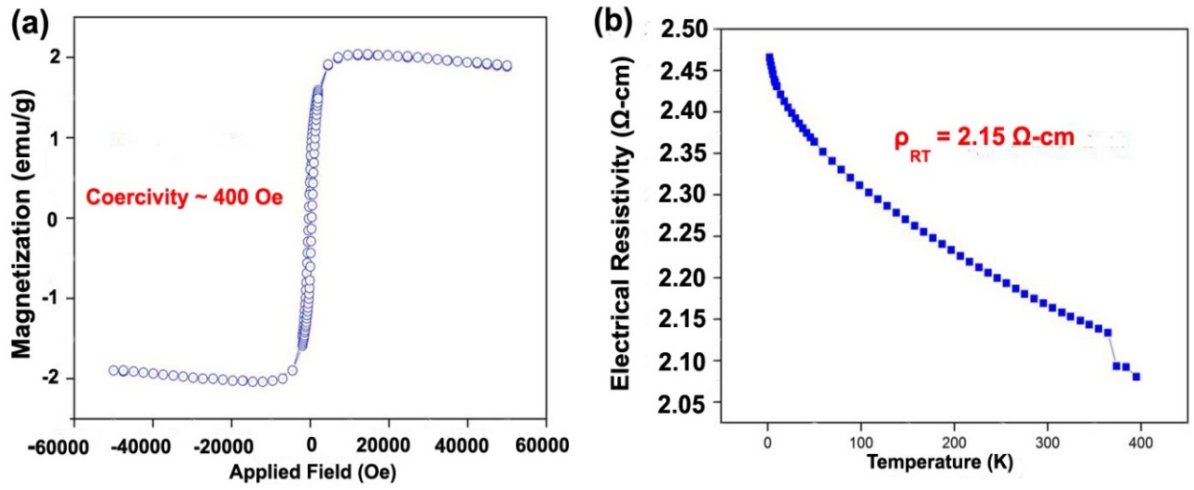

Fig. S9 Magnetization and electrical conductivity. (a) Magnetization (emu/g) versus applied magnetic field (Oe) at room temperature for the sponge, which contains small Fe catalyst particles, distributed throughout. The coercivity was found to be ~ 400 Oe; (b) PPMS four-probe electrical resistivity measurement vs. temperature of the bulk sponge material. ρ = 2.15 Ω-cm at RT. The resistivity measurement is to show it is a candidate material as a good flexible porous 3D electrode material, as mentioned in the summary of the main manuscript.

Supplementary information measurements. XRD (Fig. S2) was performed on both pristine and b-doped MWCNT samples taken under the same experimental conditions using the same Rigaku D/Max Ultima II instrument configured with Cu K-alpha radiation. Raman spectroscopy was done using a Renishaw system with laser excitation line λ = 514 nm and λ = 633 nm (Fig. S3). Four-probe electrical resistivity and magnetic moment measurements (Fig. S9) were done using a physical properties measurement system (PPMS; Quantum Design).

Supplementary Information References:

[1] Terrones, M., Grobert, N., Terrones, H. Synthetic routes to nanoscale $B_xC_yN_z$ architectures. *Carbon*, **40**, 1665–1684 (2002).

[2] Terrones, M. *et al.* New direction in nanotube science. *Materialstoday*, **7**, 30–45 (2004).

[3] Endo M., Hayashi T., Hong S-H., Enoki T., Dresselhaus, MS. Scanning tunneling microscopy study of boron-doped highly orientated pyrolytic graphite *J Appl Phys* **90**, 5670–5674 (2001).

[4] Hishiyama Y., Irumano H., Kaburagi Y., Soneda Y. Structure, Raman scattering, and transport properties of boron-doped graphite *Phys Rev B* **63,** 245406-1–11 (2001).

[5] McGuire, K. *et al.* Synthesis and Raman characterization of boron-doped single-walled carbon nanotubes. *Carbon* **43**, 219–227 (2005).

[6] Endo M. *et al.* Structural analysis of B-doped mesophase pitch-based graphite fibers by Raman spectroscopy. *Phys Rev B* **58**, 8991–8996 (1998).

[7] Liu K, Avouris P, Martel R, Hsu W. K. Electrical transport in doped multiwalled carbon nanotubes *Phys Rev B* **63**,161404–161407 (2001).

[8] Hsu W.K., Nakajima T. Electrically conductive boron-doped multi-walled carbon nanotube bundles. *Carbon* **40**, 462–465 (2002).

[9] Cancado, L. G. *et al.* Quantifying Defects in Graphene via Raman Spectroscopy at Different Excitation Energy. *Nano Lett.* **11**, 3190–3196 (2011).